

Thermodynamic phase diagram of $\text{Fe}(\text{Se}_{0.5}\text{Te}_{0.5})$ single crystals up to 28 Tesla

T. Klein^{1,2}, D. Braithwaite³, A. Demuer⁴, W. Knafo⁵, G. Lapertot³, C. Marcenat³,
P. Rodière¹, and I. Sheikin⁴, P. Strobel¹, A. Sulpice¹ and P. Toulemonde¹

¹ *Institut Néel, CNRS, 25 rue des martyrs, 38042 Grenoble, France*

² *Institut Universitaire de France and Université J.Fourier-Grenoble 1, France*

³ *SPSMS, UMR-E9001, CEA-INAC/ UJF-Grenoble 1, 17 rue des martyrs, 38054 Grenoble, France*

⁴ *LNCMI-CNRS, 25 Avenue des Martyrs, BP 166, 38042 Grenoble, France and*

⁵ *LNCMI, UPR 3228, CNRS-UJF-UPS-INSA, 31400 Toulouse, France*

(Dated: February 15, 2022)

We report on specific heat (C_p), transport, Hall probe and penetration depth measurements performed on $\text{Fe}(\text{Se}_{0.5}\text{Te}_{0.5})$ single crystals ($T_c \sim 14$ K). The thermodynamic upper critical field H_{c2} lines has been deduced from C_p measurements up to 28 T for both $H\parallel c$ and $H\parallel ab$, and compared to the lines deduced from transport measurements (up to 55 T in pulsed magnetic fields). We show that this *thermodynamic* H_{c2} line presents a very strong downward curvature for $T \rightarrow T_c$ which is not visible in transport measurements. This temperature dependence associated to an upward curvature of the field dependence of the Sommerfeld coefficient confirm that H_{c2} is limited by paramagnetic effects. Surprisingly this paramagnetic limit is visible here up to $T/T_c \sim 0.99$ (for $H\parallel ab$) which is the consequence of a very small value of the coherence length $\xi_c(0) \sim 4\text{\AA}$ (and $\xi_{ab}(0) \sim 15\text{\AA}$), confirming the strong renormalisation of the effective mass (as compared to DMFT calculations) previously observed in ARPES measurements [Phys. Rev. Lett. 104, 097002 (2010)]. H_{c1} measurements lead to $\lambda_{ab}(0) = 430 \pm 50$ nm and $\lambda_c(0) = 1600 \pm 200$ nm and the corresponding anisotropy is approximatively temperature independent (~ 4), being close to the anisotropy of H_{c2} for $T \rightarrow T_c$. The temperature dependence of both λ ($\propto T^2$) and the electronic contribution to the specific heat confirm the non conventional coupling mechanism in this system.

PACS numbers: 74.60.Ec, 74.60.Ge

I. INTRODUCTION

The discovery of superconductivity up to 55K in iron-based systems [1] has generated tremendous interest. Among those, iron selenium ($\text{FeSe}_{1-\delta}$) [2] has been reported to be superconducting with a critical temperature of 8 K at ambient pressure, rising to 34-37 K under 7-15 GPa [3]. On the other hand, the substitution of tellurium on the selenium site in $\text{Fe}_{1+\delta}(\text{Te}_x\text{Se}_{1-x})$ increases T_c to a maximum on the order of 14-15 K at ambient pressure [4, 5] (for $x \sim 0.5$). This binary compound is very interesting as it shares the most salient characteristics of iron based systems (square-planar lattice of Fe with tetrahedral coordination) but has the simplest crystallographic structure among Fe-based superconductors (no charge reservoir [6], so-called 11-structure). Moreover, even though the endpoint $\text{Fe}_{1+\delta}\text{Te}$ [7] compound displays antiferromagnetic ordering, a magnetic resonance similar to that observed in other parent compounds (with a $(1/2, 1/2)$ nesting vector connecting the Γ and M points of the Fermi surface) is recovered for intermediate Te contents [8, 9] suggesting a common mechanism for superconductivity in all iron based superconductors. However, in contrast to iron pnictides which show only weak to moderate correlations, recent ARPES measurements suggested the existence of very large mass renormalization factors (up to ~ 20 as compared to DMFT calculations) [10] indicating that $\text{Fe}(\text{Se},\text{Te})$ is a strongly correlated metal differing significantly from iron pnictides.

In order to shed light on superconductivity in these systems, it is of fundamental importance to obtain a pre-

cise determination of both upper and lower critical fields and their anisotropy. Up to now H_{c2} has mainly been deduced from transport measurements [11–13], and more recently by specific heat up to 14 T [14]. As in other pnictides (see [15] and references therein), high $H_{c2}(0)$ values have been reported but, in the case of $\text{Fe}(\text{Te}_x\text{Se}_{1-x})$, strong deviations from the standard Werthamer-Helfand-Hohenberg model for $H_{c2}(T)$ have been reported. Those deviations have been associated to paramagnetic limitations (so-called Pauli limit) [11–13]. However, in presence of strong thermal fluctuations (see discussion below), the determination of H_{c2} from transport measurement becomes very hazardous and a thorough analysis was hence lacking of an unambiguous determination of H_{c2} from specific heat measurements.

We show that the H_{c2} lines actually display a very strong downwards curvature close to T_c corresponding to $\mu_0 dH_{c2}/dT$ values rising up to ~ 12 T/K for $H\parallel c$ and even ~ 45 T/K for $H\parallel ab$. This strong curvature, not visible in transport data, shows that H_{c2} remains limited by paramagnetic effects up to temperatures very close to T_c (up to $T/T_c \sim 0.99$ for $H\parallel ab$). The corresponding Pauli field H_p is slightly anisotropic ($H_p^{\parallel ab}/H_p^{\parallel c} \sim 0.8$) whereas the orbital limit ($H_o(0)$) presents a much stronger anisotropy $H_o(0)^{\parallel ab}/H_o(0)^{\parallel c} \sim 3-4$. The huge $\mu_0 H_o(0)$ values ($\sim 130 \pm 20$ T for $H\parallel c$ and $\sim 400 \pm 50$ T for $H\parallel ab$) correspond to very small coherence length values ($\xi_{ab}(0) \sim 15 \pm 1\text{\AA}$ and $\xi_c(0) \sim 4 \pm 1\text{\AA}$) confirming the large value of the effective mass previously observed by ARPES [10] and hence supporting the presence of strong electronic correlations in this system.

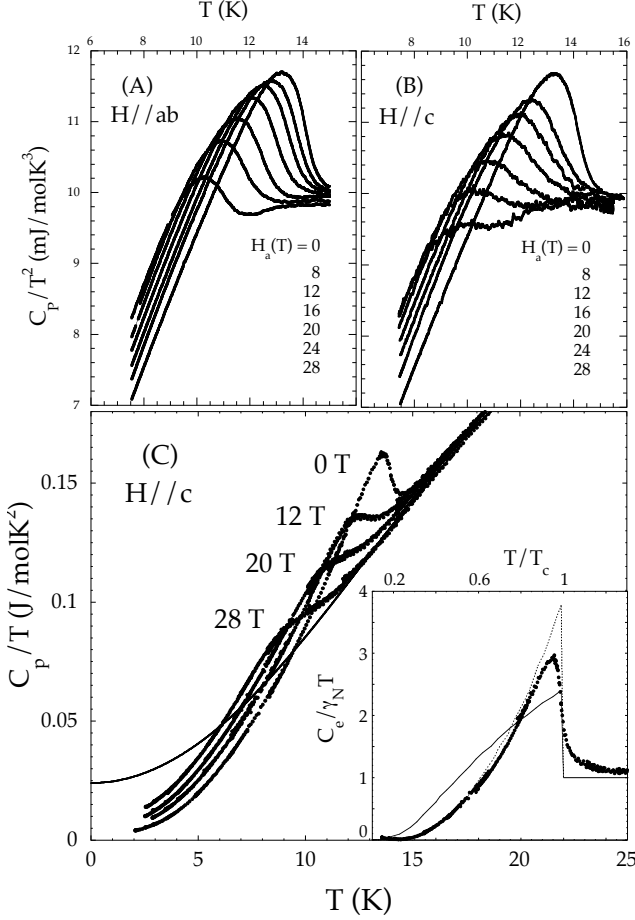


FIG. 1: AC specific heat measurements C_p/T^2 as a function of T of a $\text{Fe}(\text{Se}_{0.5}\text{Te}_{0.5})$ single crystal (sample A4) for $\mu_0 H = 0, 8, 12, 16, 20, 24$ and 28 T (from right to left) for $H \parallel ab$ (A) and $H \parallel c$ (B). The data have been renormalized taking $C_p(T = 20\text{K}) = 3.8$ J/molK. The H_{c2} line is deduced from the midpoint of the specific heat jump after subtraction of a smooth polynomial background. (C) : Specific heat from relaxation data ($H \parallel c$) for the indicated magnetic fields (sample A5). Inset : temperature dependence of the electronic contribution to the specific heat $C_e = C_p - \beta T^3 - \delta T^5$ (solid symbols) where the phonon contribution ($\beta T^3 + \delta T^5$) has been subtracted from the normal state data (see thin line in Fig.1C). The BCS behavior for $2\delta/kT_c = 3.5$ (solid line) and $2\Delta/kT_c = 5$ (dotted line) are displayed for comparison.

In addition, preliminary H_{c1} measurements led to contradictory results. On the one hand, Yadav *et al.* [16] reported on rather high H_{c1} values ~ 100 G and ~ 400 G for $H \parallel c$ and $H \parallel ab$ respectively with H_{c1} lines showing a clear upward curvature at low temperature. On the other hand, Bendele *et al.* [17] obtained much smaller values (~ 20 G and ~ 45 G for $H \parallel c$ and $H \parallel ab$ respectively) associated with a clear saturation of the $H_{c1}(T)$ lines at low temperature. Finally, Kim *et al.* [18] reported on strong deviations of the temperature dependance of the superfluid density ($\rho_s \propto 1/\lambda^2 \propto H_{c1}$) from the standard be-

havior, attributed to a clear signature of multigap superconductivity. We present here detailed first penetration field measurements performed with Hall sensor arrays in a variety of single crystals showing very different aspect ratios. We hence obtained $\mu_0 H_{c1}^{\parallel c}(0) = 78 \pm 5$ G and $\mu_0 H_{c1}^{\parallel ab}(0) = 23 \pm 3$ G. The H_{c1} lines clearly flatten off at low temperature but do not show the pronounced deep previously obtained in Tunnel Diode Oscillator (TDO) measurements [18]. Our TDO measurements however led to a similar deep which is probably due to an overestimation of the absolute $\Delta\lambda(T)$ value related to spurious edge effects. Finally, we obtained a temperature independent $\Gamma_{H_{c1}} = H_{c1}^{\parallel c}/H_{c1}^{\parallel ab}$ values $\sim 3.3 \pm 0.5$ which corresponds to $\Gamma_\lambda = \lambda_c/\lambda_{ab} \sim 4.0 \pm 0.8$ (see below), being close to the $\gamma_{H_{c2}}$ value obtained for $T \rightarrow T_c$ (i.e. $\sim H_o^{\parallel ab}/H_o^{\parallel c}$).

Finally, we confirm that $\lambda \propto T^2$ in both crystallographic directions and show that the temperature dependence of C_p strongly deviates from the standard BCS weak coupling behavior confirming the non conventional coupling mechanism of this system. However, the amplitude of the specific heat jump is much larger than those previously reported in other $\text{Fe}(\text{Se},\text{Te})$ samples and hence does not follow the ΔC_p vs T_c^3 scaling law reported in iron based systems [19, 20].

II. SAMPLE PREPARATION AND EXPERIMENTS

We present here specific heat, transport, Hall probe and Tunnel Diode Oscillator (penetration depth) measurements performed in $\text{Fe}_{1+\delta}(\text{Se}_{0.5}\text{Te}_{0.5})$ single crystals grown by two different techniques. Samples A have been grown using the sealed quartz tube method. The samples were prepared from very pure iron and tellurium pieces and selenium shots in a 1:0.5:0.5 ratio, loaded together in a quartz tube which has been sealed under vacuum. The elements were heated slowly (100°C/h) at 500°C for 10 h, then melted at 1000°C for 20h, cooled slowly down to 350°C at 5°C/h , and finally cooled faster by switching off the furnace. Single crystals were extracted mechanically from the resulting ball, the crystals being easy cleaved perpendicular to their c crystallographic axis. The refined lattice parameters of the $\text{Fe}_{1+\delta}(\text{Se}_{0.5}\text{Te}_{0.5})$ tetragonal main phase, $a = 3.7992(7)$ Å and $c = 6.033(2)$ Å, are in agreement with the literature [4, 17]. The real composition of the crystals checked by x-ray energy dispersive micro-analysis using a scanning electron microscope was found to be $\text{Fe}_{1.05(2)}(\text{Te}_{0.55(2)}\text{Se}_{0.45(2)})$. The temperature dependence of the resistivity shows a metallic behavior at low temperature as expected for this low level ($\delta = 0.05$) of interstitial iron [21].

Samples of batch B were grown with the Bridgman technique using a double wall quartz ampoule. The inside tube had a tipped bottom with a 30° angle and an open top. The inside wall of the outer ampoule was carbon coated to achieve the lowest possible oxygen par-

TABLE I: average thickness d , width w length l or mass m of the samples and measurement techniques [C_p = specific heat, R = transport, HP = Hall probe and TDO = tunnel diode oscillator]

Sample	d (μm)	w (μm)	l (μm)	measured by
A1	50	180	220	AC- C_p , HP, TDO
A2	60	300	750	HP, TDO
A3	65	400	600	HP, TDO
A3'	40	400	300	HP, TDO
A3''	40	100	100	HP, TDO
A4	$m \sim 50 \mu\text{g}$			AC- C_p
A5	$m \sim 1.1 \text{ mg}$			DC- C_p , R
B1	$m \sim 0.7 \text{ mg}$			DC- C_p , R

tial pressure during the growth. The Bridgman ampoule was inserted in a three zone gradient furnace ($1000^\circ/840^\circ/700^\circ$) and lowered at a speed of 3 mm/h. At the end of the growth, temperature was lowered to room temperature at 50° C/h . Further characterizations of these crystals have been published elsewhere [13]. The different single crystals used in this study have been listed in Table 1.

The C_p measurements have been performed in magnetic fields up to 28 T using both an AC high sensitivity technique and a conventional relaxation technique. For AC measurements, heat was supplied to the sample by a light emitting diode via an optical fiber and the corresponding temperature oscillations were recorded with a thermocouple (sample A1 and A4). In parallel, the specific heat (sample A5 and B1) were carried out in a miniaturized high-resolution micro-calorimeter using the long-relaxation technique. The chip resistance used as both thermometer and heater as well as the thermal conductance of its leads have been carefully calibrated up to 28T using a capacitance thermometer. Each relaxation provides about 1000 data points over a temperature interval of about 80% above the base temperature which has been varied between 1.8 and 20 K. Data can be recorded during heating and cooling. The merging of the upward and downward relaxation data provides a highly reliable check of the accuracy of this method.

Electrical transport measurements have been performed on sample B1 in static magnetic fields up to 28T and pulsed magnetic fields up to 55T and are described in detail elsewhere [13]. We have also measured the resistivity of sample A5 with a commercial device (PPMS) up to 9T.

The real part of the AC transmittivity, T'_H , of samples A1 to A3'' has been measured by centering these on a miniature GaAs-based quantum well Hall Sensor (of dimension $8 \times 8 \mu\text{m}^2$). The sensor is used to record the time-varying component B_{ac} of the local magnetic induction as the sample is exposed to an ac field $\sim 1 \text{ Oe}$ ($\omega \sim 210 \text{ Hz}$). T'_H is then defined as : $T'_H = [B_{ac}(T) - B_{ac}(4.2\text{K})]/[B_{ac}(T \gg T_c) - B_{ac}(4.2\text{K})]$. The remanent local DC field ($B_{rem}(H_a)$) in the sample has been measured after applying a magnetic field H_a and

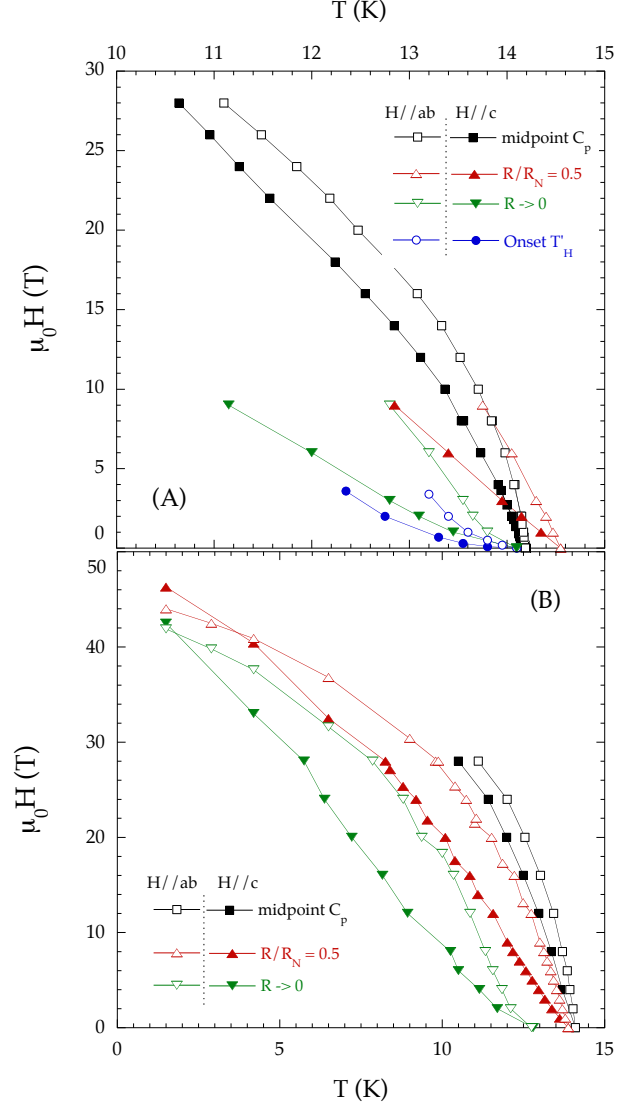


FIG. 2: (color on line) (A) $H - T$ phase diagram (batch A) in both $H \parallel ab$ (open symbols) and $H \parallel c$ (closed symbols) displaying the H_{c2} line deduced from specific heat measurements (see Fig.1)(squares), the field corresponding to the onset of the diamagnetic screening (circles) as well as the fields corresponding to zero resistance (downward triangles) and $R/R_N = 0.5$ (upward triangle, R_N being the normal state resistance). (B) same as in (A) for sample B1. The transport data are taken from [13]. See Fig.3 for a direct comparison between the H_{c2} lines in each batch.

sweeping the field back to zero. In the Meissner state, no vortices penetrate the sample and B_{rem} remains equal to zero up to $H_a = H_f$ (the first penetration field). A finite remanent field is then obtained for field amplitudes larger than H_f as vortices remain pinned in the sample.

Finally, the London magnetic penetration depth in the Meissner state, λ , has been measured on the same samples with a LC oscillating circuit (14MHz) driven by a

Tunnel Diode (TDO). The samples have been glued at the bottom of a sapphire rod which were introduced in a coil of inductance L . The variation of the penetration depth induce a change in L and hence a shift of the resonant frequency $\delta f(T) = f(T) - f(T_{min})$. $\delta f(T)$, renormalised to the frequency shift corresponding to the extraction of the sample from the coil Δf_0 is then equal to the magnetic susceptibility. At low temperatures (typically for $T \leq 12K$), $\lambda \ll d$ (d being the lowest dimension of the sample, here the thickness), and we have $\frac{\delta f(T)}{\Delta f_0} = \frac{\tilde{\lambda}}{\tilde{R}}$ where $\tilde{\lambda}$ is an effective penetration depth depending on the field orientation and \tilde{R} an effective dimension of the sample. When the magnetic field is applied along the c -axis, only the in-plane supercurrents are probed and $\tilde{\lambda} = \lambda_{ab}$, whereas $\tilde{\lambda} = \lambda_{ab} + \frac{d}{w} \lambda_c$ for $H//ab$ (w being the width of the sample). The effective dimension \tilde{R} is calculated following [22].

III. UPPER CRITICAL FIELD

Fig.1 displays typical AC measurements for both $H//c$ and $H//ab$ (sample A4). As shown, a well defined specific heat jump is obtained at T_c for $H = 0$ ($\sim 20\%$ of the total C_p) and this peak progressively shifts towards lower temperature as the magnetic field is increased (here up to 28 T). The H_{c2} line has been deduced from the midpoint of the C_p/T anomaly after subtraction of a smooth polynomial background from the raw data. As shown in Fig.2A, the corresponding H_{c2} lines present a very strong downward curvature for $T \rightarrow T_c$ which was not revealed by previous transport measurements (the same behavior is observed in all measured samples, see for instance Fig.2B and Fig.3A for a comparison between samples A4 and B1). Note that a very similar curvature has been reported very recently from C_p measurements up to 14T [14]

Such a curvature is a strong indication for paramagnetic effects and we have hence fitted the experimental data using a weak coupling BCS clean limit model including both orbital and Pauli limitations [23]. This model only requires two fitting parameters (plus T_c): the initial slope $dH_{c2}/dT|_{T=T_c}$ and the zero temperature Pauli limit H_p . The results are shown in Fig.3A for sample A4 and B1. As shown, very good fits can be obtained in both samples using very similar fitting parameters: $\mu_0 dH_{c2}/dT|_{T=T_c} \sim 38 \pm 3$ T/K and $\sim 13 \pm 2$ T/K for $H//ab$ and $H//c$ respectively and $\mu_0 H_p \sim 45 \pm 2$ T and $\sim 54 \pm 4$ T/K for $H//ab$ and $H//c$, respectively.

As previously observed in layered systems (see [24] and discussion in [25]) H_{c2}^{ab} is actually very close to a $(1 - T/T_c)^{1/2}$ law. Strikingly, this simple behaviour is valid up to $T/T_c \sim 0.99$ in our system (see Fig.3B). Such a dependence can be directly inferred from a Ginzburg-

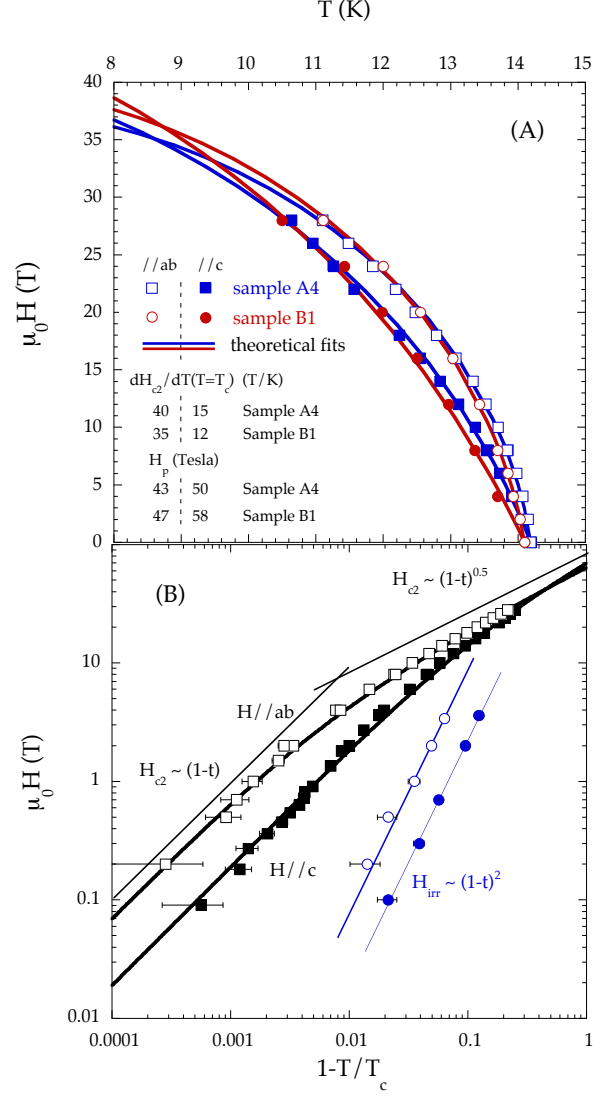


FIG. 3: (color online) (A) comparison between the $H_{c2}(T)$ values deduced from specific heat measurements in sample A4 (blue squares) and sample B1 (red circles) for both $H//c$ (closed symbols) and $H//ab$ (open symbols) and theoretical values for clean weakly coupled BCS superconductors including both orbital and Pauli limitations (solid lines). (B) H_{c2} vs $(1 - t)$ (sample A4) in a log-log scale ($t = T/T_c$) showing that the linear dependence of the H_{c2} line rapidly crosses to a $\sim (1 - t)^{0.5}$ dependence. The solid lines are fits to Eq.(1) (see text for details). The linear slopes close to T_c (~ 45 T/K and ~ 12 T/K) extrapolate to very high orbital limits. On the contrary the irreversibility line (blue circles) displays the $(1 - t)^2$ dependence characteristic of vortex melting.

Landau (GL) expansion which leads to [25]:

$$\left(\frac{H}{H_p}\right)^2 + \frac{H}{H_o} = 1 - \frac{T}{T_c} \quad (1)$$

(where H_o is the orbital field) i.e. $H_{c2} \sim H_p(1 - t)^{0.5}$ for $H \gg H_p^2/H_o$. A fit to Eq.(1) (solid line in Fig.3B) leads

to $\mu_0 H_p^{\parallel ab} \sim 65$ T and $\mu_0 H_p^{\parallel c} \sim 75$ T, $\mu_0 H_o^{\parallel ab} \sim 650$ T and $\mu_0 H_o^{\parallel c} \sim 170$ T (sample A4) [26]. We hence have $\mu_0 H_p^2/H_o \sim 6$ T for $H \parallel ab$, field which is reached for $T/T_c \sim 0.99$. Fe(Se,Te) is thus a rare example of superconductor for which the upper critical field is dominated by paramagnetic effects on almost the totality of the phase diagram (for $H \parallel ab$). As shown in Fig.3B, a linear dependence is recovered very close to T_c with $\mu_0 dH_o^{\parallel ab}/dT \sim 45$ T/K and $\mu_0 dH_o^{\parallel c}/dT \sim 12$ T/K, in good agreement with a values deduced from the BCS fitting procedure [27].

Those extremely high H_o values are related to very small values of the coherence lengths $\xi_{ab} = \Phi_0/2\pi[0.7 \times \mu_0 H_o] \sim 15 \pm 1 \text{ \AA}$ and $\xi_c = \xi_{ab} \times (H_o^{\parallel c}/H_o^{\parallel ab}) \sim 4 \pm 1 \text{ \AA}$ which confirm the very strong renormalization of the Fermi velocity observed in ARPES measurements [10] (see also theoretical calculations in [28]). Indeed, one gets $v_{F,ab} = \pi\Delta\xi_{ab}/\hbar \sim 1.4 \times 10^4$ m/s (Δ being the superconducting gap ~ 2 meV [29, 30]) i.e. $\hbar v_{F,ab} \sim 0.09$ eV\AA in perfect agreement with ARPES data which also led to $\hbar v_F \sim 0.09$ eV\AA for the α_3 hole pocket centered on the Γ point [note that the H_{c2} line will be dominated by the band having the larger critical field i.e. the lower Fermi velocity]. Our measurements do hence confirm the strong correlation effects previously suggested by ARPES measurements [10].

An estimate of the paramagnetic field in the weak coupling limit is given by the Clogston-Chandrasekhar formula : $\mu_0 H_p = 2\Delta/\sqrt{2}g\mu_B \sim 26$ T in our sample (taking $g = 2$) i.e. well below the experimental suggesting that $g \sim 1.0 - 1.2$. however, it is important to note that H_p may be increased by strong coupling effects [31] and a fit to the data can be obtained introducing an electron-phonon coupling constant $\lambda \sim 0.6 - 0.7$ and $g \sim 2$ (still having an anisotropy on the order of 1.2 between the two main crystallographic axis). Even if it is difficult to conclude on the exact value of g , our data clearly indicate a small anisotropy of this coefficient (~ 1.2) supporting the possibility of a crossing of the H_{c2} lines at low temperature. Note that this anisotropy is much lower than the one inferred from transport measurements (~ 4 [13]) confirming that the large apparent anisotropy of g deduced from those measurements is an artifact, probably related to the anisotropy of flux dynamics (see discussion on the irreversibility line below). The anisotropy of the upper critical field is then strongly temperature dependent rising from $H_{c2}^{ab}/H_{c2}^c \sim H_p^{ab}/H_p^c \sim 0.8$ for $T \rightarrow 0$, reflecting the small anisotropy of the g factor, to $H_{c2}^{ab}/H_{c2}^c \sim H_o^{ab}/H_o^c \sim 3.5 - 4$ close to T_c , reflecting the anisotropy of the coherence lengths (see Fig.7).

IV. IRREVERSIBILITY LINE

The small ξ values associated to large λ values ($\lambda_{ab}(0) \sim 430$ nm (see below and [17]) lead to strong fluctuation effects hindering any direct determination of

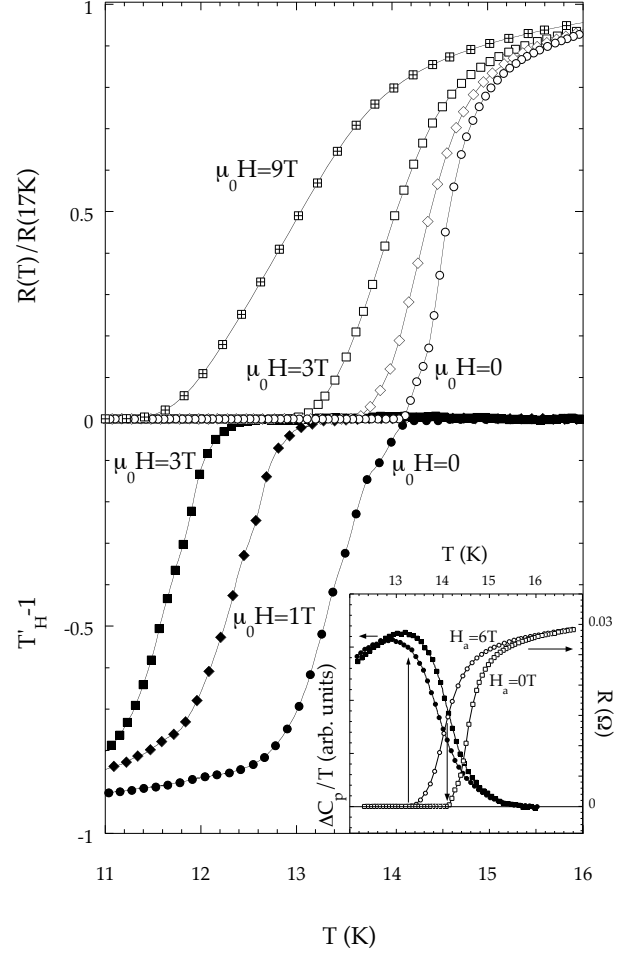


FIG. 4: Transport and AC transmittivity measurements as a function of T for the indicated magnetic fields ($H \parallel c$) in Fe(Se_{0.5},Te_{0.5}) single crystals. In the inset : comparison between transport and specific heat data for $\mu_0 H = 0$ and 6 T ($\parallel c$) emphasizing that the midpoint of the specific heat anomaly does not correspond to any characteristic temperature in $R(T)$ for $H \neq 0$.

H_{c2} from either transport or susceptibility measurements. These fluctuations can be quantified by the Ginzburg number $G_i = (k_B T_c / \epsilon_0 \xi_c)^2 / 8$ where $\epsilon_0 (= (\Phi_0 / 4\pi \lambda_{ab})^2)$ is the line tension of the vortex matter. One hence obtains $\epsilon_0 \xi_c \sim 40$ K (as a comparison $\epsilon_0 \xi_c \sim 200$ K in cuprates) and $G_i \sim 10^{-2}$ which is very similar to the value obtained in YBa₂Cu₃O_{7- δ} or NdAsFe(O_{1-x}F_x) (so called 1111-phase, see [32] and references therein) clearly showing that thermal fluctuations are very strong in this system.

To emphasize this point, we have reported in Fig.2, the temperatures corresponding to both $R \rightarrow 0$ and $R/R_N = 0.5$ deduced from transport measurements up to 9T for sample A4 (see also Fig.4) and even up to 50T for sample B1 (see [13]) (R_N being the normal state resistance). As shown, none of those lines present the strong

downward curvature obtained in C_p measurements. On the contrary, the $R/R_N = 0$ lines vary almost linearly with T with $d\mu_0 H/dT \sim 11$ T/K and ~ 5 T/K for $H\parallel ab$ and $H\parallel c$, respectively in agreement with previous measurements [11, 12]. However, as pointed above, these lines do not correspond to any thermodynamic criterion and discussions of the corresponding lines should hence be taken with great caution. Moreover whereas the mid-point of the specific heat coincides with the $R = 0$ temperature for $H = 0$ in sample A4, this midpoint rather lies close to the $R/R_N = 0.5$ point in sample B1 clearly showing that neither of those two transport criteria can be associated with the H_{c2} line.

Similarly, as previously observed in high temperature cuprates and 1111-pnictides [32], the onset of the diamagnetic response ($T'_H \rightarrow 0$) also lies well below the H_{c2} line. (see Fig.2A and Fig.4). Indeed, this onset is related to the irreversibility line above which the system is unable to screen the applied AC field due to the free motion of vortices. This irreversibility line is then expected to lie close to the $R = 0$ line. As shown in Fig.4 the onset of diamagnetism actually differs slightly from the onset of resistivity. This difference is much probably related to different voltage-current criteria (the magnetic screening corresponds to much smaller electric fields but requires higher currents) but both lines present the positive curvature characteristic of the onset of irreversible processes. Note that, as expected for vortex melting (for a review see [33]), the irreversibility line (here defined as the onset of T'_H) varies as : $H_{irr} \propto (1 - T/T_c)^\alpha$ with $\alpha \sim 2$ (see Fig.3B). A similar curvature has also been reported by Bendele *al.* [17] for the irreversibility field deduced from magnetization measurements.

V. LOWER CRITICAL FIELD

The first penetration field has been measured on a series of $\text{Fe}(\text{Se}_{0.5}\text{Te}_{0.5})$ samples with very different aspect ratios (see Table 1). To avoid spurious effects associated to strong pinning preventing the vortex diffusion to the center of the sample [34] H_f has also been measured on several locations of the same sample. The inset of Fig.5 displays typical examples on sample A3' (2 positions) and A3". In samples with rectangular cross sections, flux lines partially penetrate into the sample through the sharp corners even for $H_a < H_f$ but remain "pinned" at the sample equator. The magnetization at $H_a = H_f$ is then larger than H_{c1} and the standard "elliptical" correction for H_{c1} ($= H_f/(1 - N)$ where N is the demagnetization factor) can not be used anymore. Following [35], in presence of geometrical barriers, H_f is related to H_{c1} through :

$$H_{c1} \approx \frac{H_f}{\tanh(\sqrt{\alpha d/w})} \quad (2)$$

where α varies from 0.36 in strips to 0.67 in disks (d and w being the thickness and width of the sample, respec-

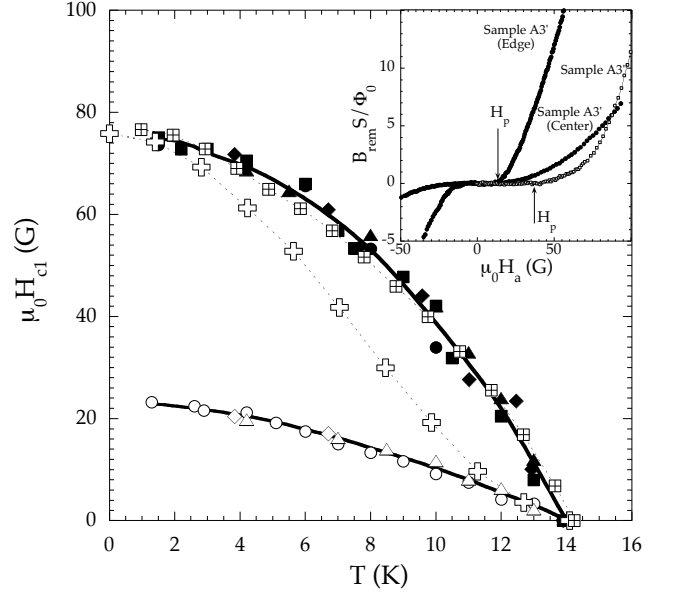


FIG. 5: Temperature dependence of the lower critical field (H_{c1}) deduced from Hall probe measurements for $H\parallel ab$ (open symbols) and $H\parallel c$ (closed symbols) in sample A1 (squares), A2 (circles), A3 (lozenges) and A3'' (triangles), see Table 1 for sample dimensions. Solid lines are guides to the eyes, crossed squares are muon relaxation data from [23] and open crosses TDO data. In the inset : remanent field B_{rem} as a function of the applied field in sample A3' (center and edge) and A3''.

tively. To reduce the uncertainty associated with the α value as well as the d/w ratio in real samples of irregular shape, five different samples with different aspect ratios have been measured (see Table 1). Sample A3' has been cut out of sample A3 and finally A3'' out of A3' in order to directly check the influence of the aspect ratio on H_f . The corresponding H_f values are reported in the inset of Fig.7 together with the theoretical predictions from Eq.(2) taking $\mu_0 H_{c1}^{ab} = 78$ G (the predictions for a standard "elliptical" correction are also displayed for comparison).

The lower critical fields ($\mu_0 H_{c1}^c$, $\mu_0 H_{c1}^{ab}$) are then related to the penetration depth (λ_c , λ_{ab}) through :

$$\mu_0 H_{c1}^c = \frac{\Phi_0}{4\pi\lambda_{ab}^2} (Ln(\kappa) + c(\kappa)) \quad (3)$$

$$\mu_0 H_{c1}^{ab} = \frac{\Phi_0}{4\pi\lambda_{ab}\lambda_c} (Ln(\kappa^*) + c(\kappa^*)) \quad (4)$$

where $\kappa = \lambda_{ab}/\xi_{ab}$, $\kappa^* = \lambda_c/\xi_{ab}$ and $c(\kappa)$ is a κ dependent function tending towards ~ 0.5 for large κ values. Taking $\mu_0 H_{c2}(0) = 0.7 \times \mu_0 H_o \sim 130$ T, and $H_{c1}^c = 78 \pm 5$ G one gets $\lambda_{ab}(0) \sim 430 \pm 50$ nm, which is in fair agreement with muons relaxation data [17, 36]. This very large λ value confirms the general trend previously inferred in iron pnictides (see for instance [17] and references therein) pointing towards a linear increase of T_c vs $1/\lambda_{ab}^2$ as in-

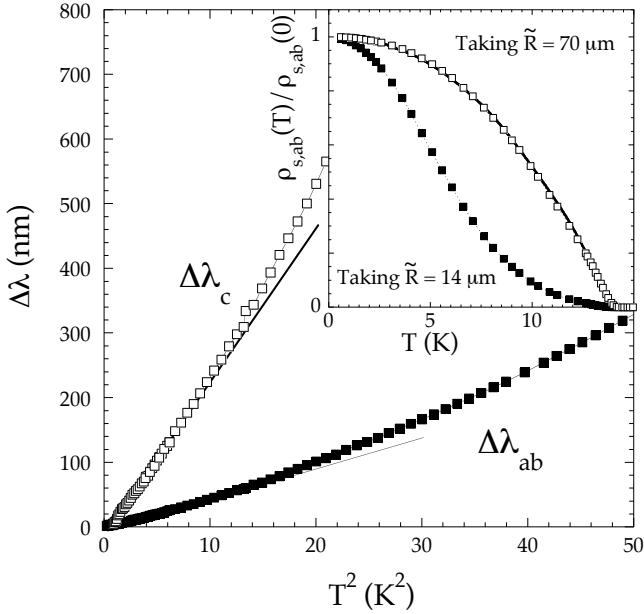


FIG. 6: Temperature dependence of λ_{ab} (solid symbols) and λ_c (open symbols) deduced from the frequency shift in TDO measurements (sample A3'', Table 1). Inset : temperature dependence of the superfluid density $\rho_S^{TDO}(T)/\rho_S^{TDO}(0) = 1/(1 + \Delta\lambda_{ab}(T)/\lambda_{ab}(0))^2$ taking $\lambda_{ab}(0) = 430$ nm and $\tilde{R} = 14\mu\text{m}$ (solid symbols) (i.e. following [22]), see corresponding $\Delta\lambda_{ab}(T)$ values on the main panel) or $\tilde{R} = 70\mu\text{m}$ (open symbols). The average $H_{c1}(T)/H_{c1}(0)$ curve (see Fig.5) is displayed as the thick solid line.

tially proposed in cuprates by Uemura *et al.* [37]. For $H\parallel ab$, no correction was introduced (flat samples) and one hence obtains $\mu_0 H_{c1}^{ab} = \mu_0 H_f^{ab} = 23 \pm 3$ G leading to $\lambda_c \sim 1600 \pm 200$ nm (taking $\mu_0 H_{c2}^{ab} = 0.7 \times \mu_0 H_o^{ab} \sim 460$ T)

As shown in Fig.5, $H_{c1}(T)$ clearly shows a saturation at low temperature. As a comparison we have reported on Fig.5 the temperature dependence of the superfluid density deduced from muons relaxation data [36] and $\rho_S^{TDO}(T)$ measurements [18]. Both H_{c1} and $\rho_S^{\mu SR}(T)$ curves are similar but do not reproduce the important shoulder at 5 K of the superfluid density. This shoulder has been interpreted as a clear signature of multi-gap superconductivity and as a failure of the clean limit s-wave (including $s\pm$) pairing [18]. Our measurements do not support this interpretation.

In order to shed light on this discrepancy, we have performed TDO measurements on each of the samples of Table 1. As described in sec.II, λ_c and λ_{ab} were deduced from the effective penetration depth $\tilde{\lambda}$ measured for both $H\parallel ab$ and $H\parallel c$. As shown in Fig.6 (sample A3''), both $\Delta\lambda_{ab}$ and $\Delta\lambda_c$ are proportional to T^n with n close to 2, in good agreement with previous measurements for $H\parallel c$ [18] (the same temperature dependence has been

obtained for all samples). The TDO data then require the introduction of the value of $\lambda_{ab}(0)$ to convert the $\Delta\lambda(T)$ data into $\rho_S^{TDO}(T)/\rho_S^{TDO}(0) = 1/(1 + \Delta\lambda_{ab}(T)/\lambda_{ab}(0))^2$. Introducing $\lambda_{ab}(0) \sim 430\text{nm}$ and taking $\tilde{R} \sim 14\mu\text{m}$ (from [22]), $\rho_S^{TDO}(T)$ shows a change of curvature around 5K, very similar to the one previously reported in [18] (see inset of Fig.6). A similar discrepancy has already been observed in MgCNi_3 and interpreted as a reduction of the critical temperature at the surface of the sample due to a modification of the carbon stoichiometry [38]. However, such an explanation is not expected to hold here as single crystals were extracted mechanically from the bulk.

It is important to note that the temperature dependence of the superfluid density is very sensitive to the absolute value of $\Delta\lambda$ and, although very similar to the one reported by Kim *et al.* [18], the amplitude of $\Delta\lambda_{ab}/T^2 \sim 40\text{\AA}/\text{K}^2$ observed in our samples is much larger than the one reported recently by Sarafin *et al.* [14] ($\sim 10\text{\AA}/\text{K}^2$). Similar discrepancies in the absolute amplitude of $\Delta\lambda$ have also been reported in other pnictides [39] and have been attributed to complications from rough edges which may lead to an overestimation of $\Delta\lambda$. Dividing the absolute $\Delta\lambda_{ab}$ by a factor ~ 5 (i.e. taking $\tilde{R} = 70\mu\text{m}$ for $H\parallel c$ instead of $14\mu\text{m}$) actually leads to a very good agreement between TDO and H_{c1} data (see Fig.6) hence indicating that this value has probably been overestimated due to an underestimation of the effective dimension \tilde{R} in presence of rough edges.

Very similar temperature dependences of H_{c1} were obtained in both directions (see Fig.5) leading to a (almost) temperature independent anisotropy of H_{c1} : $\Gamma_{H_{c1}} \sim 3.4 \pm 0.5$ and hence $\Gamma_\lambda = \lambda_c/\lambda_{ab} = [H_{c1}^c/H_{c1}^{ab}] \times [(Ln(\kappa^*) + c(\kappa))/(Ln(\kappa^*) + c(\kappa))] \sim \Gamma_{H_{c1}} \times 1.2 \sim 4.1 \pm 0.8$ (see Fig. 7). This value is hence very close to the one obtained for H_{c2} close to T_c as $\Gamma_{H_{c2}}(T \rightarrow T_c) \sim \Gamma_{H_o} = \xi_{ab}/\xi_c$ (see Fig.7). Similarly, very similar temperature dependences have been obtained for $\Delta\lambda_c$ and $\Delta\lambda_{ab}$ (with $\Delta\lambda_c \sim 5 \times \Delta\lambda_{ab}$ up to $T \sim T_c$) again suggesting a weak temperature dependence of this anisotropy. Finally, this value is also close to the one obtained for the irreversibility field deduced from the onset of diamagnetic screening.

VI. FINAL DISCUSSION

The value of the normal state Sommerfeld coefficient (γ_N) in $\text{Fe}(\text{Se},\text{Te})$ compounds remains debated as values ranging from ~ 23 mJ/molK² [40] to ~ 39 mJ/molK² [4] have been obtained. For non superconducting samples, it has even been shown recently [41] that γ_N rises rapidly for $x < 0.1$ reaching ~ 55 mJ/molK² for $0.1 \leq x \leq 0.3$. Even though our maximum field (28 T) is too low to fully destroy superconductivity down to 0 K hence hindering any precise determination of γ_N , it is worth noting that a γ_N value on the order of ~ 39 mJ/molK² is incompatible with the entropy conservation rule in our sample. A reasonable fit to the data (solid line in Fig.1C) assuming that $C_p/T = \gamma_N + \beta T^2 + \delta T^4$ for $20 > T > 12$ K

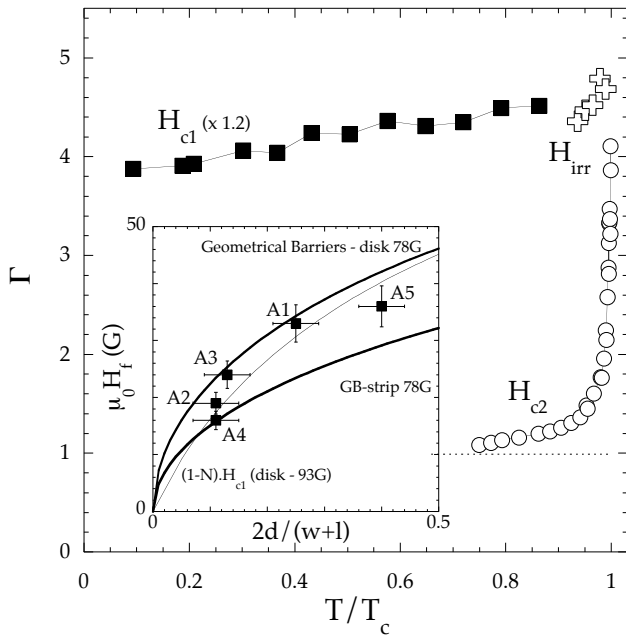


FIG. 7: Temperature dependence of the anisotropy of the upper (open circles), and lower (solid squares) critical fields and irreversibility line (onset of diamagnetic response, open crosses). The $\Gamma_{H_{c1}}$ data have been multiplied by a factor 1.2 to display $\Gamma_\lambda = 1.2 \times \Gamma_{H_{c1}}$. In the inset : first penetration field H_f as a function of the aspect ratio : $2d/(w+l)$. Thick solid lines are theoretical predictions in presence of geometrical barriers using see Eq.(2) for disks (upper line) and strips (lower line); the thin line correspond to a standard "elliptical" correction (no surface barrier).

and $\mu_0 H = 28$ T leads to $\gamma_N = 23 \pm 3$ mJ/molK² in good agreement with the value obtained by Tsurkan *et al.* [40]. This γ_N value is also in fair agreement with the one deduced from ARPES measurements (~ 30 mJ/molK² [10]). Similarly, the Debye temperature ($\Theta_D \sim 143$ K) is in reasonable agreement with the one previously reported in both Fe(Se_{0.67}Te_{0.23}) ($\Theta_D \sim 174$ K [4]) and Fe_{1.05}Te ($\Theta_D \sim 141$ K [42]).

The electronic contribution to the specific heat ($C_e/T = C_p/T - \beta T^2 - \delta T^4$) is then displayed in the inset of Fig.1 together with the theoretical prediction for a single gap BCS superconductor in the weak coupling limit (i.e. taking $2\Delta/kT_c \sim 3.5$, thin solid line). As shown, this standard behavior largely overestimates the experimental data at low temperature suggesting the presence of a much larger gap. A reasonable agreement to the data is obtained assuming that $2\Delta/kT_c \sim 5$ (dotted line). However, even though some indication for the presence of a large gap were obtained by fitting either μSR [36] or optical conductivity [43] data, the corresponding gap value (~ 3 meV) is much larger than the value obtained by spectroscopy ($\sim 1.8 - 2$ meV [29, 30]). Moreover those former measurements also suggest the presence

of a much smaller gap which is not present in our specific heat measurements.

Some evidence for nodes (or for deep gap minima) in Fe(Se_{0.5}Te_{0.5}) has been suggested by four fold oscillations in the low temperature specific heat for $H||c$ [45]. However, despite the high resolution of our AC technique and the very good quality of our samples (the specific heat jump at T_c is slightly larger than in [45]) we did not observe these oscillations in our samples (i.e. $\Delta C_p(\theta)/C_p < 10^{-3}$). Nodes are also expected to show up in the field dependence of the Sommerfeld coefficient ($\gamma(H)$) which is then expected to vary as H^α with $\alpha < 1$ ($\alpha = 0.5$ for the so-called Volovik effect for d-wave pairing with line nodes whereas $\alpha \sim 1$ for classical single gap BCS systems). We have hence extrapolated the $C_e(H)/T$ data to zero using either a BCS formula (see discussion above, $C_e/T - \gamma(H) \propto \exp(-\Delta(H)/kT)$ in our temperature range) or a phenomenological second order polynomial fit. Both procedure led to a *concave* curvature for $\gamma(H)$ with $\alpha \sim 1.5 \pm 0.3$ for $H||c$ and $\alpha \sim 2.2 \pm 0.6$ for $H||ab$. This concave behavior can be attributed to the effect of Pauli paramagnetism on the vortex cores [46] (see [47, 48] for experimental data in heavy fermions) hence clearly supporting the importance of these effects in Fe(Se_{0.5}Te_{0.5}).

Finally note that it has been suggested that $\Delta C_p/T_c$ could be proportional to T_c^2 in iron pnictides [19, 20] due to strong pair breaking effects [49] with $\Delta C_p/T_c^3 \sim 0.06$ mJ/molK⁴. One hence would expect an anomaly $\Delta C_p/T_c \sim 12$ mJ/molK² at T_c in our system which is clearly lower than the experimental value $\sim 40 \pm 5$ mJ/molK². Similarly, it has been suggested that the initial slope of the H_{c2} line could scale as $\mu_0 dH_{c2}/dT \sim 0.2 \times T_c$ (T/K) but, again, this scaling does not hold in our sample for which $\mu_0 dH_{c2}/dT \sim 12$ T/K. Finally note that the temperature dependence of the superfluid density (see discussion above) supports the $\Delta\lambda_{ab}/T^2 \sim 10 \text{ \AA}^2/\text{K}^2$ value obtained by Serafin *et al.* [14] which is also much smaller than the one suggested from the scaling of [50] : $\Delta\lambda_{ab}/T^2 \sim 8.8 \times 10^4/T_c^3 \sim 32 \text{ \AA}^2/\text{K}^2$.

VII. CONCLUSION

In summary,

(i) Precise determinations of the H_{c2} lines from C_p measurements led to a very strong downward curvature, similar to that observed in layered systems.

(ii) The temperature dependence of the upper critical field and the field dependence of the Sommerfeld coefficient both indicate that H_{c2} is limited by strong paramagnetic effects with $\mu_0 H_p \sim 45 \pm 2$ T and $\sim 54 \pm 4$ T for $H||ab$ and $H||c$, respectively.

(iii) The very small value of the coherence length $\xi_{ab}(0) \sim 15 \text{ \AA}$ confirms the strong renormalisation of the effective mass (compared to DMFT calculations) previously observed in ARPES measurements [10] and associated strong electron correlation effects. γ_N is estimated

to $\sim 23 \pm 3$ mJ/molK² in fair agreement with the ARPES value.

(iv) The anisotropy of the orbital critical field is estimated to be on the order of 4 hence leading to a $\xi_c(0)$ value smaller than the c lattice parameter.

(v) Neither the temperature dependence of λ nor that of the electronic contribution to the specific heat follow the weak coupling BCS model (an BCS dependence with $\Delta/kT_c \sim 5$ remains possible) but no evidence for nodes in the gap is obtained from the field dependence of the Sommerfeld coefficient. We did not observe the fourfold oscillations of the low temperature specific heat previously obtained by Zeng *et al.* [45].

(vi) The amplitude of the specific heat jump $\Delta C_P/T_c \sim 40 \pm 5$ mJ/molK² is much larger than that previously observed in Fe(Se,Te) and does not follow the $\Delta C_P/T_c^3$ inferred in iron pnictides. Similarly neither the slope of the H_{c2} line nor the absolute value of $\Delta\lambda(T)$ obey the scaling laws previously proposed for iron pnictides [49, 50].

(vii) $\lambda_{ab}(0) = 430 \pm 50$ nm and $\lambda_c(0) = 1600 \pm 200$ nm, confirming the very small superfluid density previously observed in iron pnictides. The corresponding anisotropy

is almost temperature independent with $\Gamma_\lambda \sim \Gamma_{H_{c2}}(T \rightarrow T_c) = \gamma_\xi$.

(viii) These large λ values associated to small ξ values lead to a very small condensation energy $\epsilon_0 \xi_c \sim 40$ K and hence to large fluctuation effects hindering any determination of H_{c2} from either transport or susceptibility measurements. A detailed analysis of the influence of these fluctuations on the specific heat anomaly will be presented elsewhere.

(ix) The strong upward curvature of the irreversibility line (defined as the onset of diamagnetic screening) : $H_{irr} \propto (1 - T/T_c)^2$ strongly suggests the existence of a vortex liquid in this system.

This work has been supported by the French National Research Agency, Grant ANR-09Blanc-0211 SupraTetrafer and ANR 'DELICE', and by the Euromagnet II grant via the EU co tract RII-CT-2004-506239. TK is most obliged to V. Mosser of ITRON, Montrouge, and M.Konczykowski from the Laboratoire des Solides Irradiés, Palaiseau for the development of the Hall sensors used in this study. We thank J-P.Brisson for the software used to fit the H_{c2} data.

-
- [1] Y. Kamihara, T. Watanabe, M. Hirano, and H. Hosono, J. Am. Chem. Soc. **130**, 3296 (2008); X. H. Chen, T. Wu, G. Wu, R. H. Liu, H. Chen, and D. F. Fang, Nature London **453**, 761 (2008).
 - [2] F. C. Hsu, J. Y. Luo, K. W. Yeh, T. K. Chen, T. W. Huang, P. M. Wu, Y. C. Lee, Y. L. Huang, Y. Y. Chu, D. C. Yan, and M. K. Wu, Proc. Natl. Acad. Sci. U.S.A, **105**, 14262 (2008).
 - [3] Garbarino *et al.* Euro. Phys. Lett. **86**, 27001(2009); Medvedev *et al.* Nature Mat. **8**, 630 (2009); Margadonna *et al.* Phys. Rev. B **80**, 064506 (2009); Mizuguchi *et al.* Applied Phys. Lett. **93**, 152505 (2008), Braithwaite *et al.* J. Phys.: Condens. Matter **21**, 232202 (2009).
 - [4] B. C. Sales, A. S. Sefat, M. A. McGuire, R. Y. Jin, D. Mandrus, and Y. Mozharivskyj, Phys. Rev. B **79**, 094521 (2009).
 - [5] K.-W. Yeh, T. W. Huang, Y. L. Huang, T. K. Chen, F. C. Hsu, P. M. Wu, Y. C. Lee, Y. Y. Chu, C. L. Chen, J. Y. Luo, D. C. Yan, and M. K. Wu, Europhys. Lett. **84**, 37002 (2008); M. H. Fang, H. M. Pham, B. Qian, T. J. Liu, E. K. Vehstedt, Y. Liu, L. Spinu, and Z. Q. Mao, Phys. Rev. B, **78**, 224503 (2008).
 - [6] Assuming that the additional iron atoms siting on Fe2 sites between the Se/Te atoms do not constitute a charge reservoir.
 - [7] Wei Bao, Y. Qiu, Q. Huang, M. A. Green, P. Zajdel, M. R. Fitzsimmons, M. Zhernenkov, S. Chang, M. Fang, B. Qian, E. K. Vehstedt, Jinhu Yang, H. M. Pham, L. Spinu, and Z. Q. Mao, Phys. Rev. Lett. **102**, 247001 (2009).
 - [8] Y. Qiu, W. Bao, Y. Zhao, C. Broholm, V. Stanev, Z. Tesanovic, Y. C. Gasparovic, S. Chang, Jin Hu, Bin Qian, M. Fang, and Z. Mao, Phys. Rev. Lett. **103**, 067008 (2009); M. D. Lumsden, A. D. Christianson, E. A. Goremychkin, S. E. Nagler, H. A. Mook, M. B. Stone, D. L. Abernathy, T. Guidi, G. J. MacDougall, C. de la Cruz, A. S. Sefat, M. A. McGuire, B. C. Sales and D. Mandrus, Nature Physics, **6**, 182 (2010).
 - [9] A. Martinelli, A. Palenzona, M. Tropeano, C. Ferdeghini, M. Putti, M. R. Cimberle, T. D. Nguyen, M. Affronte, and C. Ritter, Phys. Rev. B, **81**, 094115 (2010).
 - [10] A. Tamai, A.Y. Ganin, E. Rozbicki, J. Bacsá, W. Meevasana, P. D. C. King, M. Caffio, R. Schaub, S. Margadonna, K. Prassides, M. J. Rosseinsky, and F. Baumberger, Phys. Rev. Lett. **104**, 097002 (2010).
 - [11] H. Lei, R. Hu, E. S. Choi, J. B. Warren, and C. Petrovic, Phys. Rev. B, **81**, 094518, (2010); T. Kida, T. Matsunaga, M. Hagiwara, Y. Mizuguchi, Y. Takano, and K. Kindo, J. Phys. Soc. Jpn **78**, 113701 (2009).
 - [12] M. H. Fang, J. H. Yang, F. F. Balakirev, Y. Kohama, J. Singleton, B. Qian, Z. Q. Mao, H. D. Wang, H. Q. Yuan, Phys. Rev. B **81**, 020509 (2010)
 - [13] D. Braithwaite, G. Lapertot, W. Knafo, I. Sheikin, J. Phys. Soc. Jpn **79**, 053703 (2010).
 - [14] A. Serafin, A. I. Coldea, A.Y. Ganin, M.J. Rosseinsky, K. Prassides, D. Vignolles, and A. Carrington, Phys. Rev. B, **82**, 104514 (2010).
 - [15] Pribulova, T. Klein, J. Kacmarcik, C. Marcenat, M. Konczykowski, S. L. Budko, M. Tillman, and P. C. Canfield Phys. Rev. B **79**, 020508 (2009).
 - [16] C.S. Yadav, P.L. Paulose, New Journal of Physics **11**, 103046 (2009).
 - [17] M. Bendele, S. Weyeneth, R. Puzniak, A. Maisuradze, E. Pomjakushina, K. Conder, V. Pomjakushin, H. Luetkens, S. Katrych, A. Wisniewski, R. Khasanov, and H. Keller, Phys. Rev. B, **81**, 224520 (2010).
 - [18] H. Kim, C. Martin, R. T. Gordon, M. A. Tanatar, J. Hu, B. Qian, Z. Q. Mao, Rongwei Hu, C. Petrovic, N. Salovich, R. Giannetta, and R. Prozorov, Phys. Rev. B,

- 81**, 180503(R), (2010).
- [19] S. L. Budko, Ni Ni, and P. C. Canfield, Phys. Rev. B **79**, 220516(R) (2009).
- [20] J. Paglione and R. L. Greene, Nat. Phys. **6**, 645 (2010).
- [21] T. J. Liu, X. Ke, B. Qian, J. Hu, D. Fobes, E. K. Vehstedt, H. Pham, J. H. Yang, M. H. Fang, L. Spinu, P. Schiffer, Y. Liu, and Z. Q. Mao, Phys. Rev. B **80**, 174509 (2009).
- [22] R. Prozorov and R. W. Giannetta Superconductor Science and Technology **19**, R41 (2006).
- [23] J. P. Brison, N. Keller, A. Verniere, P. Lejay, L. Schmidt, A. Buzdin, J. Flouquet, S. R. Julian, and G. G. Lonzarich: Physica C **250** (1995) 128.
- [24] S. T. Ruggiero, T. W. Barbee and M. R. Beasley, Phys. Rev. Lett. **49**, 1299 (1980); C. Uher, J. L. Cohn and I. K. Schuller, Phys. Rev. B, **34**, 4906 (1986).
- [25] S. I. Vedenev, C. Proust, V. P. Mineev, M. Nardone, and G. L. J. A. Rikken, Phys. Rev. B, **73**, 014528 (2006).
- [26] note that the the zero temperature extrapolations of the fields deduced from GL expansions always overestimate the experimental values.
- [27] Note that we could expect to observe a dimensional crossover at a temperature T^* for which $\xi_c(T^*) \sim c/\sqrt{2}$ with $H_{c2}^{ab} = \sqrt{3}\Phi_0/\pi d\xi_{ab} \propto (1 - T/T_c)^{0.5}$ for $T < T^*$ (taking $\xi_{ab} = \xi_{ab}(0) \times (1 - T/T_c)^{-0.5}$). This crossover is however hindered by the Pauli field $H_p \ll H_{c2}^{2D} \sim 2600 \times (1 - T/T_c)^{0.5}$.
- [28] M. Aichhorn, S. Biermann, T. Miyake, A. Georges, and M. Imada, Phys. Rev. B, **82**, 064504 (2010).
- [29] T. Hanaguri, S. Niitaka, K. Kuroki, H. Takagi, Science **328**, 474 (2010).
- [30] T. Kato, Y. Mizuguchi, H. Nakamura, T. Machida, H. Sakata, and Y. Takano, Phys. Rev. B, **80**, 180507(R) (2009).
- [31] H_p is expected to be enhanced by a factor $\eta(1 + \lambda_{e-ph})^\epsilon$ in the strong coupling limit where λ_{e-ph} is the electron-phonon coupling constant and ϵ is an exponent ranging from 0.5 (T. P. Orlando *et al.* Phys. Rev. B **19**, 4545 (1979) to 1 (M. Schossmann and J. P. Carbotte, Phys. Rev. B **39**, 4210 (1989).
- [32] J. Kacmarcik, C. Marcenat, T. Klein, Z. Pribulova, M. Konczykowski, S. L. Budko, M. Tillman, N. Ni and P. C. Canfield, Phys. Rev. B, **80**, 014515 (2009).
- [33] G. Blatter, M. V. Feigelman, V. B. Geskenbein, A. I. Larkin, and V. M. Vinokur, Rev. Mod. Phys. **66**, 1125 (1994).
- [34] R. Okazaki, M. Konczykowski, C. J. van der Beek, T. Kato, K. Hashimoto, M. Shimozaawa, H. Shishido, M. Yamashita, M. Ishikado, H. Kito, A. Iyo, H. Eisaki, S. Shamoto, T. Shibauchi, I and Y. Matsuda, Phys. Rev. B, **79**, 064520 (2009).
- [35] E. H. Brandt Phys. Rev. B **59**, 3369 (1999).
- [36] P. K. Biswas, G. Balakrishnan, D. M. Paul, C. V. Tomy,, M. R. Lees, I and A. D. Hillier, Phys. Rev. B, **81**, 092510 (2010).
- [37] J. Uemura, G. M. Luke, B. J. Sternlieb, J. H. Brewer, J. F. Carolan, W. N. Hardy, R. Kadono, J. R. Kempton, R. F. Kiefl, S. R. Kreitzman, P. Mulhern, T. M. Riseman, D. Li, Williams, B. X. Yang, S. Uchida, H. Takagi, J. Gopalakrishnan, A. W. Sleight, M. A. Subramanian, C. L. Chien, M. Z. Cieplak, G. Xiao, V. Y. Lee, B. W. Statt, C. E. Stronach, W. J. Kossler, and X. H. Yu, Phys. Rev. Lett. **62**, 2317 (1989).
- [38] P. Diener, P. Rodière, T. Klein, C. Marcenat, J. Kacmarcik, Z. Pribulova, D. J. Jang, H. S. Lee, H. G. Lee, and S. I. Lee, Phys. Rev. B **79**, 220508 (2009).
- [39] K. Hashimoto, A. Serafin, S. Tonegawa, R. Katsumata, R. Okazaki, T. Saito, H. Fukazawa, Y. Kohori, K. Kihou, C. H. Lee, A. Iyo, H. Eisaki, H. Ikeda, Y. Matsuda, A. Carrington, and T. Shibauchi, Phys. Rev. B **82**, 014526 (2010).
- [40] V. Tsurkan, J. Deisenhofer, A. Gunther, C. Kant, H.-A. Krug von Nidda, F. Schrettle, and A. Loidl, cond-mat arXiv: 1006.4453v1.
- [41] T. J. Liu, J. Hu, B. Qian, D. Fobes, Z. Q. Mao, W. Bao, M. Reehuis, S. A. J. Kimber, K. Prokes, S. Matas, D. N. Argyriou, A. Hiess, A. Rotaru, H. Pham, L. Spinu, Y. Qiu, V. Thampy, A. T. Savici, J. A. Rodriguez and C. Broholm, Nat. Mat. **9**, 716 (2010).
- [42] G. F. Chen, Z. G. Chen, J. Dong, W. Z. Hu, G. Li, X. D. Zhang, P. Zheng, J. L. Luo, and N. L. Wang, Phys. Rev. B, **79**, 140509(R) (2009).
- [43] C. C. Homes, A. Akrap, J. S. Wen, Z. J. Xu, Z. W. Lin, Q. Li, and G. D. Gu, Phys. Rev. B **81**, 180508 (2010).
- [44] note that the zero field curve extrapolates towards a very small but non zero value which can be attributed to the presence of a small fraction of parasitic phase.
- [45] B. Zeng, G. Mu, H. Q. Luo, T. Xiang, H. Yang, L. Shan, C. Ren, I. I. Mazin, P. C. Dai and H.-H. Wen, cond-mat arXiv:1007.3597v1.
- [46] H. Adachi, M. Ichide, K. Machidaz, J. Phys. Soc. Jpn **74** 2181 (2005); M. Ichida and K. Machida, Phys. Rev. B, **76** 064502 (2007).
- [47] H. Aoki, T. Sakakibara, H. Shishido, R. Settai, Y. Onuki, P. Miranovi, and K. Machida, J. Phys. Condens. Matter **16**, L13 (2004); K. Deguchi, S. Yonezawa, S. Nakatsuji, Z. Fisk, and Y. Maeno, J. Magn. Magn. Mater. **310**, 587 (2007).
- [48] S. Nishizaki, Y. Maeno and Z. Mao, Journal of the Phys. Soc. of Jpn. **69**, 572 (2000).
- [49] V. G. Kogan, Phys. Rev. B **80**, 214532 (2009).
- [50] R. T. Gordon, H. Kim, M. A. Tanatar, R. Prozorov, and V. G. Kogan, Phys. Rev. B, **81**, 180501(R) (2010).